

Robust Hypothesis Tests for Detecting Statistical Evidence of 2D and 3D Interactions in Single-Molecule Measurements

Christopher P. Calderon ^{†,*}, Lucien E. Weiss [‡], and W. E. Moerner [‡]

[†] *Numerica Corporation, Loveland, Colorado, 80538 and*

[‡] *Department of Chemistry, Stanford University, Stanford, California, 94305.*

(Dated: May 29, 2022)

A variety of experimental techniques have improved the 2D and 3D spatial resolution that can be extracted from *in vivo* single-molecule measurements. This enables researchers to quantitatively infer the magnitude and directionality of forces experienced by biomolecules in their native cellular environments. Situations where such forces are biologically relevant range from mitosis to directed transport of protein cargo along cytoskeletal structures. Models commonly applied to quantify single-molecule dynamics assume that effective forces and velocity in the x, y (or x, y, z) directions are statistically independent, but this assumption is physically unrealistic in many situations. We present a hypothesis testing approach capable of determining if there is evidence of statistical dependence between positional coordinates in experimentally measured trajectories; if the hypothesis of independence between spatial coordinates is rejected, then a new model accounting for 2D (3D) interactions should be considered to more faithfully represent the underlying experimental kinetics. The technique is robust in the sense that 2D (3D) interactions can be detected via statistical hypothesis testing even if there is substantial inconsistency between the physical particle’s actual noise sources and the simplified model’s assumed noise structure. For example, 2D (3D) interactions can be reliably detected even if the researcher assumes normal diffusion, but the experimental data experiences “anomalous diffusion” and/or is subjected to a measurement noise characterized by a distribution differing from that assumed by the fitted model. The approach is demonstrated on control simulations and on experimental data (IFT88 directed transport in the primary cilium).

PACS numbers: 87.80.Nj, 87.10.Mn, 05.40.Jc, 2.50.Tt, 5.45.Tp

I. INTRODUCTION

Several advances in optical microscopy have increased the spatial and temporal resolution that can be extracted from single particle tracking (SPT) experiments. For example, the techniques used in Refs. [1–9] enable researchers to experimentally monitor the 2D (or 3D) kinetics of a fluorescently tagged biomolecule *in vivo*. However, commonly used SPT analysis techniques do not explicitly model 2D or 3D spatial interactions despite the fact that spatially dependent force interactions or anisotropic diffusion can be important in many biological processes including intracellular trafficking [8], diffusion in confined environments [9], molecular motor induced transport [6], chromatin dynamics [10], and mitosis [11].

Recent articles related to SPT analysis methods have studied 2D/3D estimation [12–14] and goodness-of-fit (GoF) testing [14] (i.e., checking the consistency of model assumptions against individual experimental trajectories containing thermal and measurement noise). GoF tests are helpful in checking the various statistical assumptions implied by an assumed model, but GoF tests looking for non-specific model imperfections are not always desirable in SPT data analysis. For example, suppose a researcher observes a 2D time series generated by an SPT experiment (positions of the tagged particle are denoted by x and y) and subsequently uses this to estimate the pa-

rameters of a standard diffusion, but the underlying data is generated by a process with anomalous diffusion (i.e., $H \neq \frac{1}{2}$ where H is the Hurst exponent [15–20]). If a GoF test is used and the model is rejected, the GoF test would not directly reveal the specific reason for rejection [14, 21]. In this example, the incorrect thermal noise model would ultimately lead to rejection by a consistent GoF test regardless of whether or not unmodeled statistical dependence exists between the x and y coordinates.

In situations where a researcher is solely interested in determining if statistically significant evidence of 2D or 3D interactions exists in the experimental data, he/she may want to specifically test for any dependence between x, y (or x, y, z) measurements. It would be desirable to have such a hypothesis test be robust to questionable modeling assumptions which can be challenging to test in short SPT trajectories containing both thermal fluctuations and noise induced by the measurement apparatus. For example, the anomalous vs. standard diffusion question can be hard to resolve using a single trajectory when one only has access to a time series spanning $\approx 1 - 5$ s and measurement noise is significant relative to thermal fluctuations [18–20] (this noise is sometimes referred to as “localization noise” [22] in the SPT literature). Robustness against questionable localization noise assumptions is desirable since this noise is difficult to accurately quantify in many experiments [14, 22–24] despite its potential heavy influence on parameter estimation, hypothesis testing, and other model diagnostics [25–27]. In addition, methods not requiring ensemble averaging (i.e., those capable of carrying out tests with a

* chris.calderon@numerica.us

single trajectory) are of interest since the effective dynamics experienced *in vivo* can be heterogeneous due to varying local micro-environments [14, 19, 20].

In this work, we present such a hypothesis testing technique. This is accomplished by combining techniques discussed in Refs. [14] and [28]. Practical utility of the approach is demonstrated through both simulation and experiments. Although we focus on situations motivated by SPT experiments, the techniques are applicable to other single-molecule experiments involving 2D (or 3D) time series measurements.

II. METHODS

A. Data Generating Process (DGP) Used in Simulation Studies

For the simulation cases studied, a stochastic differential equation (SDE) model of the form:

$$d\vec{r}_t = \frac{\sigma\sigma^T}{k_B T} F \vec{r}_t dt + \sqrt{2\sigma} d\vec{B}_t^H \quad (1)$$

$$\vec{\psi}_k = \vec{r}_k + \vec{\epsilon}_k, \quad (2)$$

is used as the data generating process (DGP). In the expression above, $\vec{r}_t \in \mathbb{R}^d$ denotes the position of the tagged particle (e.g., if $d = 2$ then $r = (x, y)^T$ where T denotes the transpose operation); $k_B T$ is the product of Boltzmann's constant and temperature; the product of $F \in \mathbb{R}^{d \times d}$ and \vec{r}_t determines the instantaneous force experienced by the particle; \vec{B}_t^H is a fractional Brownian motion (fBm) [16, 19, 20] [29]; and $\vec{\psi}_k$ is the measurement/observation vector taken at time t_k . Note that the position is not directly observed due experimental artifacts like localization noise [18, 22]; the latter is modeled a mean zero Gaussian noise $\vec{\epsilon}_k$ having covariance R . Both σ and R are diagonal matrices $\in \mathbb{R}^{d \times d}$. To specify the model parameters, we report possible nonzero elements of matrices; for example, if $d = 2$, then F will have four parameters ($F_{11}, F_{21}, F_{12}, F_{22}$) and R will have two (R_{11}, R_{22}) where subscripts denote rows/columns.

B. Model and Hypothesis Testing Procedure Outline

To model observations, the multivariate SDEs (with $H = \frac{1}{2}$) presented in Ref. [14] are utilized. This assumed model structure allows one to utilize exact Kalman filter likelihood equations for both estimation and inference. After applying maximum likelihood estimation (MLE), one can use the estimated MLE parameter, the model's implied conditional distribution, and the time series observations ($\{\psi_k\}_{k=1}^N$) to generate the normalized innovation sequence $\{\vec{e}_k\}_{k=1}^N$ [14]. In what follows (using notation from Ref. [28]), components of the estimated normalized innovation vector, \vec{e}_k , are denoted by e_{jk} where

the first subscript indexes the position coordinate and the second subscript indexes time.

In Ref. [14], the components of different coordinates were combined into a single time series, e.g. a one dimension vector of the form $(e_{11}, e_{21}, e_{31}, e_{12}, e_{22}, \dots, e_{3N})$ was constructed for each MLE; subsequently, the GoF tests reported in Ref. [30] were utilized. The problem with this approach is that temporal and spatial measurement information is aggregated together. This can result in a loss of power in detecting model imperfections caused by time dependent interactions between different spatial coordinates. Furthermore, Hong and Li's tests are GoF tests seeking to detect any model imperfection (some modeling errors may not be of scientific interest).

The methods of Duchesne *et al.* focus on tests that depend on the empirical rank statistics of estimated residuals [28] (in our situation, the residuals are the normalized innovations [27]). Duchesne *et al.*'s approach utilizes a multivariate time series analysis approach applicable to two or more components (technical complications associated with testing time series vectors in \mathbb{R}^3 are readily handled [28]). The multivariate approach respects the natural time and space ordering of the raw observations (in contrast the GoF approach used in Ref. [27] where a $d = 3$ vector was collapsed to a $d = 1$ vector as illustrated in the previous paragraph). To achieve this, Duchesne *et al.* developed a technique that uses the so-called Möbius transformation to map a collection of empirical distributions to a collection of asymptotically independent Gaussian random variables under the null hypothesis of independence.

In this study, we compute \mathcal{H}_N (the generalized cross correlation statistic discussed in Ref. [28]) to test for dependence. We also study the related Cramer-von Mises test statistic, \mathcal{W}_N [28]. The Appendix summarizes and discusses the equations originally presented in Ref. [28] that we utilize in this work. Note that we study multiple test statistics for both GoF and independence testing since selecting the "best" test statistic in finite sample sizes where spatial and/or temporal dependence exists in the observational data can be difficult [21].

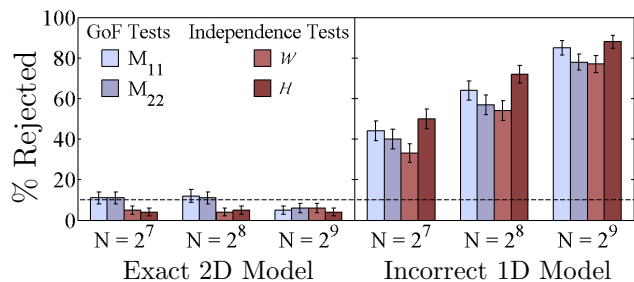


FIG. 1. (Color online). Percent rejections obtained with four test statistics applied to two models (vertical lines denote error bars). Dashed horizontal line displays expected percent rejection under null and infinite sample sizes. (Left) 2D model with $H = \frac{1}{2}$ and correlation (induced by F) matching the DGP. (Right) Incorrect 1D model neglecting statistical dependence.

C. Simulation Parameters

In all cases studied, the trajectory observations are $\{\vec{\psi}_k\}_{k=1}^N$ where 10 *ms* separate observations and the system temperature is 310 K. For the simulations, 400 Monte Carlo trajectories were used to estimate MLEs and test statistics. The SDE parameters are: $F = (-4, -2, -1, -1) [\frac{pN}{\mu m}]$, $\sigma = (.2, .3) [\frac{\mu m}{s^{1/2}}]$, $R = (30, 20) [nm]$ for the 2D simulations and $F = (-4, -2, 0, -1, -1, .1, 0, 0 - .1) [\frac{pN}{\mu m}]$, $\sigma = (.2, .3, .3) [\frac{\mu m}{s^{1/2}}]$, $R = (30, 20, 20) [nm]$ for 3D.

D. Experimental Details

IFT88-eYFP tracking experiments in live cultured cells [31] were performed using an Olympus IX-71 inverted microscope with a 100x, 1.4 NA oil objective (UPLSAPO, Olympus). Cell culture was performed as previously described [32]. Two days prior to experiments, cells were detached (Invitrogen, TripLE Express) from cell culture dishes (Thermo Scientific, tissue culture treated 10 cm dish) and replated onto cell-culture filters (Corning, Costar Transwell 0.4 μm Polyester Membrane 6.5 mm Inserts) in low-serum DMEM media (Thermo, 0.5% Hyclone Fetal Bovine Serum; Invitrogen, Gibco phenol red-free Dulbecco's Modified Eagle Medium) to induce cilia growth. At the start of the experiment, filters were placed onto #1 glass coverslips (Fisher) and contained in a humidity and temperature controlled stage-top incubator (Tokai-Hit, ONICS). The sample was illuminated with circularly polarized, 514 nm pumping light (Coherent Sapphire, 50 mW). Fluorescence collected through the objective was filtered with a dichroic beamsplitter (Semrock, FF425/532/656-Di01) and a bandpass filter (Semrock, FF01-578/105-25) before being imaged in 10 ms frames on an electron multiplied charge-coupled device (Andor Technology, iXon Ultra DU897). Single-molecule trajectories were gathered from the subsequent movie using custom Matlab image-analysis software that fit a 2D symmetric Gaussian with a constant offset to a small region of the image. Bad fits were removed if the fitted parameters were determined to be inconsistent with those of a single YFP molecule.

III. RESULTS

The results are divided into two sections. The first presents the (unrealistic) situation where one of the assumed stochastic models precisely matches the DGP (i.e., all noise distributions and spatial/temporal dependencies are exactly known). The second set of results shows the more practical situation where the DGP has features not accounted for in the fitted model. GoF procedures and hypothesis tests aiming to detect unmodeled statistical dependence are studied in both situations.

A. Control Simulations: *The DGP Matches an Assumed Model*

In Fig. 1, a 2D SDE with $H = \frac{1}{2}$ and correlation between x and y serves as the DGP. Here and in what follows, “correlated” refers to dependence induced by non-zero off-diagonal terms in F and “uncorrelated” refers to situations where F is a diagonal matrix. Two models are applied to each simulated trajectory. One estimated model, referred to as “2D SDE” has the correct parametric structure; the other model constrains the off-diagonal entries of F to be zero resulting in an uncorrelated model (this model is also referred to as the “1D SDE” since one estimate model parameters without jointly observing x and y). For each trajectory, the MLE parameter is computed (see Ref. [14]) along with four tests statistic \mathcal{W}_N , \mathcal{H}_N , $M(1, 1)$, and $M(2, 2)$; the first two test statistics aim to robustly detect unmodeled statistical dependence [28] and the latter two check GoF [30]; these four test statistics are computed for each individual trajectory. The fraction of rejections are plotted for various N (nominal expected rejection rate under the null hypotheses shown by dashed horizontal line). Table I contains analogous results, except a 3D SDE with $H = \frac{1}{2}$ generates data. These results demonstrate the Type I error rate and power under situations and sample sizes relevant to various SPT applications. Note that \mathcal{H}_N improves power in detecting 2D/3D interactions in the cases studied (comparable power improvement also occurs if the 3D simulations in Ref. [14] are studied).

TABLE I. Hypothesis Testing Results with 3D Data Generating Process. Fraction rejected using nominal Type I rate = 10%. For the (incorrect) 1D model, off-diagonal entries of F are set to 0.

	Exact 3D Model				1D Model			
N	\mathcal{W}	\mathcal{H}	M_{11}	M_{22}	\mathcal{W}	\mathcal{H}	M_{11}	M_{22}
2^8	10.3	9.3	5.5	7.0	25.3	32.3	21.5	16.3
2^9	9.0	9.5	6.3	6.8	43.0	58.0	40.3	33.8

B. Robustness Studies: *The DGP Does Not Match Assumed Model*

Next we turn to situations where the DGP does not match the assumed model. The previously studied 2D DGP is modified to have $H = 0.74$ [16]; note that σ is multiplied by 250 to keep trajectories comparable, the remaining SDE parameters are identical. The $H > \frac{1}{2}$ case was studied because measurement noise can significantly complicate detection of artifacts induced by thermal noise with $H < \frac{1}{2}$ in the “high frequency” and relatively small N sampling regime studied [18, 26]. Fig. 2 demonstrates that the GoF tests are able to detect the long range correlation in noise (and the unmodeled spatial correlation). The dependence test for \mathcal{W}_N and \mathcal{H}_N are just above the nominal null threshold in the 2D SDE

model (unmodeled statistical dependence between x and y is again readily detected in the 1D SDE model). Although the (incorrect) 2D SDE model with $H = \frac{1}{2}$ is able to remove much of the linear correlation, statistical dependence between the residuals (e_{1k} and e_{2k}) still exists due to the actual DGP having $H = 0.74$; as more data is obtained, it becomes easier to detect this dependence, hence rejection rates are above the nominal null level even in the 2D model.

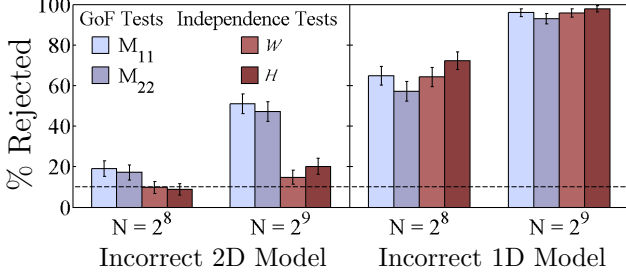


FIG. 2. (Color online) DGP uses correlated anomalous diffusion, with $H = .74$. Both models incorrectly assume normal ($H = \frac{1}{2}$) diffusion. 2D model allows for correlation; 1D model sets correlation to zero.

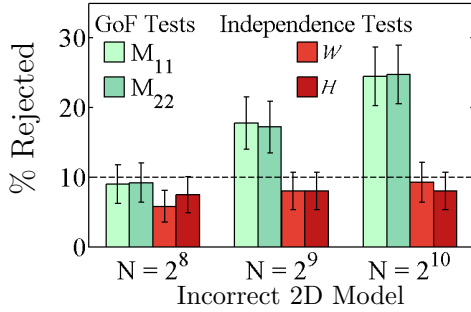


FIG. 3. (Color online) DGP uses uncorrelated anomalous diffusion, with $H = .74$. New coloring scheme emphasizes that no statistical dependence exists between x and y in the DGP. Incorrect 2D model allows for potential correlation (but uses incorrect H). The GoF Tests detect signatures of $H = 0.74$ whereas the Independence Tests (correctly) achieve the expected rejection under null (null of the latter tests is consistent with the DGP).

To demonstrate that the method of Ref. [28] is robust to an incorrectly assumed model where no x/y dependence exists, the previous DGP is modified to have off-diagonal terms of F set to zero. The same model and test statistics are applied, but now there is truly no statistical dependence. Fig. 3 shows the 2D SDE model (assuming $H = \frac{1}{2}$) achieves the expected rejection rates for the null hypothesis (the GoF tests still detect artifacts of $H \neq \frac{1}{2}$).

Figure 4 provides another illustration of robustness. In this situation, the DGP process is once again the correlated 2D standard diffusion studied in Sec. III A, but the fitted 2D SDE model constrains R to zero (the other parameters are fit via MLE). Recall that in the DGP, the diagonal terms in R are greater than zero (hence mea-

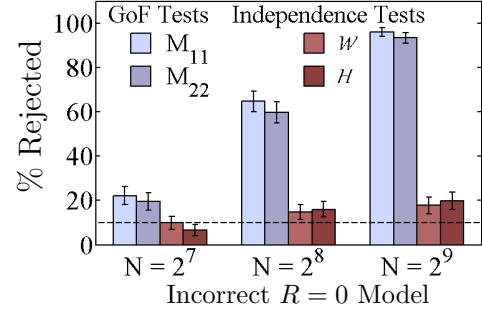


FIG. 4. (Color online) DGP uses correlated standard diffusion with measurement noise. The 2D model allows for potential correlation in the drift, but incorrectly assumes no measurement noise is present (i.e., the model sets $R = 0$ without estimating this parameter from observed data). The GoF Tests readily detect signatures of $R > 0$ in the data. The Independence Tests are relatively robust to the modeling error, but the innovations are not statistically independent due to measurement noise modeling errors (see discussion in main text).

surement noise is known to be present). The GoF tests readily detect the modeling error induced by setting R equal to zero for all N considered. The independence tests reject relatively close to the nominal null level since statistical dependence induced by F is accounted for explicitly. However, measurement noise that is not properly modeled can cause non-Markovian effects. For example, increments of observations are anti-correlated in many situations relevant to SPT analysis [18, 22, 25, 26]. The coupling induced by non-zero off diagonal components in F of the DGP causes the normalized innovations (computed using the fitted model obtained where R is set to zero) to become statistically dependent and this effect just starts to become detectable for the larger N studied. Making F diagonal removes this effect (results not shown, but are similar to those shown in Fig. 3). Note that we took the extreme case of setting $R = 0$, so other experimental artifacts affecting the localization noise distribution, e.g. [14, 22, 33–36], should also be readily handled by the independence testing approach discussed in this work.

C. Illustration of How the Assumed Stochastic Model Affects Statistical Power

Although we just demonstrated robustness, this does not imply that all models detect dependence between x and y with equal power. Fig. 5 uses the same DGP as in 1, but fits a models where F is set to zero and all other parameters are estimated (i.e., the “Zero Drift Model”). Neglecting to account for the linear autocorrelation induced by diagonal components of F substantially reduces the power of \mathcal{W}_N and \mathcal{H}_N ; the unmodeled autocorrelation dominates the signal in the empirical marginals and complicates detecting dependence between x and y . Hence, when aiming to detect statistical dependence, we

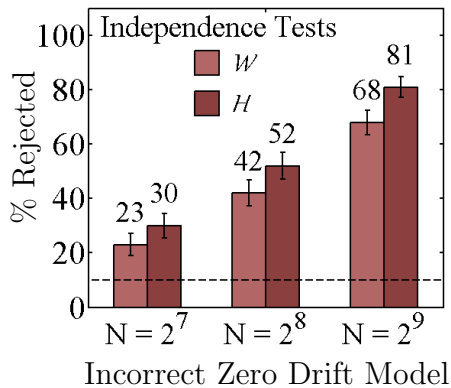


FIG. 5. (Color online). Same as Fig. 1 except the assumed model sets all drift parameters equal to zero. Note: $\mathcal{W} = 33, 54, 77\%$ and $\mathcal{H} = 50, 72, 88\%$ for the 1D Model studied in Fig. 1.

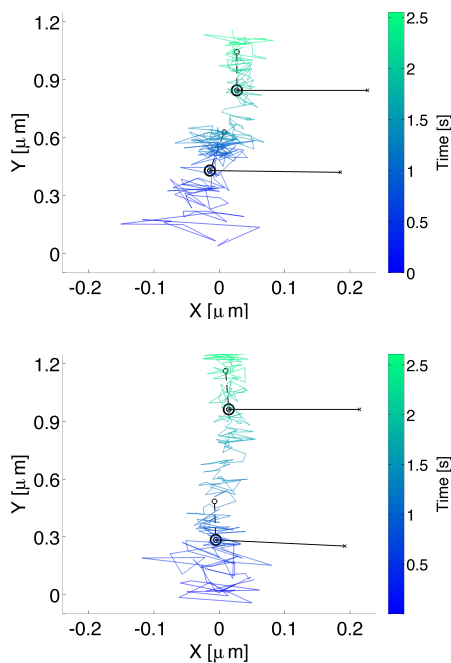


FIG. 6. (Color online). YFP tagged IFT88 trajectories in the primary cilium of live epithelial cells. Top: case where rejection caused by curved track occurred with $N = 2^8$ points (p -vals of 2D and 1D models < 0.05). Bottom: case where straight line motion was not rejected with $N = 2^8$. The arrows plotted denote the estimated eigenvectors of F obtained by dividing the data into two disjoint time windows of size $N = 2^7$ (eigenvectors corresponding to larger magnitude eigenvalue denoted by dark solid lines).

suggest using estimation schemes advocated in Ref. [14] since these models nest many classic SPT models as special cases.

D. Application to Experimental IFT88 Trajectories

Finally, we apply the techniques to analyze the IFT88 data described in the Methods section. Fig. 6 plots two trajectories where the molecular motors on IFT88 move cargo through the primary cilium [9]. The total number of data points plotted corresponds to $N = 2^8$; in the top panel, the cytoskeletal track is curved and both 1D and 2D models assuming a constant F are rejected using \mathcal{H}_N with $N = 2^8$. In the bottom panel, the directed motion is effectively along a “straight line” and the constant F 2D model is not rejected by \mathcal{H}_N or \mathcal{W}_N with $N = 2^8$. We subsequently divided the trajectories into two disjoint time series of size $N = 2^7$ and extracted the MLE of the 2D models; the arrows in the plots show the eigenvectors corresponding to the estimated F (the eigenvectors show the natural local coordinates). For the $N = 2^7$, no tests applied resulted in rejection. The fact that the estimated eigenvector “align” with the direction of motion also suggests the $N = 2^7$ is adequate to provide a local linear approximation of the curved cytoskeletal track. These trajectories provide a clean graphical example of nontrivial statistical dependence between measured x, y positions. The technique presented detected unmodeled dependence in a nonstationary signal containing thermal and measurement noise, however, other nonlinear dependencies (beyond curvature) can be detected with the approach advocated in Ref. [28].

IV. CONCLUSIONS

Hypothesis tests for detecting statistical dependence between measured x, y (z) data were demonstrated on simulated and experimental SPT data. The approach was shown to be robust to controversial assumptions (e.g., anomalous vs. normal diffusion) and exhibited reasonable power when presented single trajectories with small N and non-negligible measurement noise using parameters characteristic of SPT experiments. The measurement noise issue is particularly relevant to SPT applications since complex background and other optics effects can complicate reliably modeling and extracting parameters characterizing noise induced by the measurement apparatus [14, 22, 33–36]. Such effects often become more pronounced as the temporal resolution increases [26], so the “robustness” aspect of the testing procedure shown is particularly appealing from an applied experimental data analysis perspective.

V. ACKNOWLEDGMENTS

The authors thank L. Milenkovic and M.P. Scott for experimental help and K. Ghoudi for sharing code illustrating an efficient computational implementation of the 3D method presented in Ref. [28]. CPC’s work was supported by NSF SBIR Grant No. 1314897; LEW &

WEM's by NIH Grant No. R01GM086196 and a Stanford Bio-X Graduate Student Fellowship.

VI. APPENDIX

The Möbius transformation for the test of primary interest in our study is defined by:

$$\mathbb{R}_{A,\vec{\ell},N}(\vec{x}) = N^{-\frac{1}{2}} \sum_{k=1}^N \prod_{j \in A} [\mathbb{I}\{e_{j,k+l_j} \leq x_j\} - F_{jN}(x_j)], \quad (3)$$

$$F_{jN}(e_{j,t+l_j}) := \frac{1}{N} \sum_{k=1}^N \mathbb{I}\{e_{jk} \leq e_{j,k+l_j}\}. \quad (4)$$

In the expression above, $\mathbb{I}\{\cdot\}$ represents the indicator function of an event; $\vec{\ell}$ specifies a temporal offset (or “time lag” [28]) vector; x_j (l_j) is component j of $\vec{x} \in \mathbb{R}^d$ ($\vec{\ell} \in \mathbb{R}^d$); and F_{jN} denotes the empirical marginal distribution of residual j estimated from N observations [28]. The set A is a collection of position indices (e.g., $A = (1, 3)$ represents the x and z coordinates). Let \mathcal{A} denote the collection of all possible spatial interactions, e.g. if $d = 3$ then $\mathcal{A} = \{(1, 2, 3), (1, 2), (1, 3), (2, 3)\}$. Despite the fact that $\mathbb{R}_{A,\vec{\ell},N}$ and $\mathbb{R}_{B,\vec{\ell},N}$ for $A, B \in \mathcal{A}$ can have overlapping empirical rank information, the Möbius transformation (Eq. 3) has the property that $\text{cov}(\mathbb{R}_{A,\vec{\ell},N}, \mathbb{R}_{B,\vec{\ell},N}) = 0$ unless $A = B$ and $\vec{\ell} = \vec{\ell}'$ in

the limit $N \rightarrow \infty$ (additional transformations can produce standard Gaussian vectors [28]); these fact can be exploited to construct test statistics generated by combining multiple lag vectors ($\vec{\ell}$) and position index sets (A) into a single test statistic.

As mentioned in the main text, we are primarily interested in the generalized cross-correlations. This quantity is defined by:

$$\begin{aligned} N^{\frac{1}{2}} \hat{\gamma}_{A,\vec{\ell},N} &= (-1)^{|A|} \int_{\mathbb{R}^{|A|}} \mathbb{R}_{A,\vec{\ell},N}(\vec{x}^{(A)}) d\vec{x}^{(A)} \\ &= N^{-\frac{1}{2}} \sum_{k=1}^N \prod_{j \in A} (e_{j,k+l_j} - \bar{e}_j) \end{aligned} \quad (5)$$

where $|A|$ is the number of elements in A , $\vec{x}^{(A)}$ are the coordinates of \vec{x} contained in A , and $\bar{e}_j := \frac{1}{N} \sum_{k=1}^N e_{j,k}$. The second line above follows from the definition of $\mathbb{R}_{A,\vec{\ell},N}$ and the fact that the mean of a continuous random variable X (having distribution function $F(t) := P(X \leq t)$) is given by $\mathbb{E}[X] = \int_0^\infty (1 - F(t)) dt - \int_{-\infty}^0 F(t) dt$ for real-valued random variables [37] (the multivariate analog of this identity is used above [28]). In our work, we use the same time lag parameter vectors utilized in Ref. [28] throughout. The primary test statistic of interest, \mathcal{H}_N , is readily computed using these expressions (the relevant expressions for \mathcal{W}_N are provided in Ref. [28]).

-
- [1] Arhel, N., Genovesio, A., Kim, K., Miko, S., Perret, E., Olivo-Marin, J., Shorte, S., and Charneau, P. *Nat. Methods* **3**(10), 817–824 (2006).
 - [2] Golding, I. and Cox, E. *Phys. Rev. Lett.* **96**(9), 14–17 March (2006).
 - [3] Lessard, G. A., Goodwin, P. M., and Werner, J. H. *Appl. Phys. Lett.* **91**(22), 224106 November (2007).
 - [4] Lange, S., Katayama, Y., Schmid, M., Burkacko, O., Bräuchle, C., Lamb, D. C., and Jansen, R.-P. *Traffic* **9**(8), 1256–67 August (2008).
 - [5] Manley, S., Gillette, J., Patterson, G., Shroff, H., Hess, H., Betzig, E., and Lippincott-Schwartz, J. *Nat. Methods* **5**(2), 155–157 (2008).
 - [6] Thompson, M. A., Casolari, J. M., Badieirostami, M., Brown, P. O., and Moerner, W. E. *Proc. Natl. Acad. Sci. U. S. A.* **107**(42), 17864–71 October (2010).
 - [7] Weigel, A. V., Simon, B., Tamkun, M. M., and Krapf, D. *Proc. Natl. Acad. Sci. U. S. A.* **108**(16), 6438–43 April (2011).
 - [8] Ram, S., Kim, D., Ober, R. J., and Ward, E. S. *Biophys. J.* **103**(7), 1594–603 October (2012).
 - [9] Ye, F., Breslow, D. K., Koslover, E. F., Spakowitz, A. J., Nelson, W. J., and Nachury, M. V. *Elife* **2**, e00654 (2013).
 - [10] Verdaasdonk, J. S., Vasquez, P. A., Barry, R. M., Barry, T., Goodwin, S., Forest, M. G., and Bloom, K. *Mol. Cell* (2013).
 - [11] Stephens, A. D., Snider, C. E., Haase, J., Haggerty, R. a., Vasquez, P. a., Forest, M. G., and Bloom, K. *J. Cell Biol.* **203**(3), 407–16 November (2013).
 - [12] Masson, J., Casanova, D., Turkcan, S., Voisinne, G., Popoff, M., Vergassola, M., and Alexandrou, A. *Phys. Rev. Lett.* **102**(4), 48103 (2009).
 - [13] Voisinne, G., Alexandrou, A., and Masson, J.-B. *Biophys. J.* **98**(4), 596–605 February (2010).
 - [14] Calderon, C. P., Thompson, M. A., Casolari, J. M., Paffenroth, R. C., and Moerner, W. E. *J. Phys. Chem. B* October (2013).
 - [15] Kou, S. and Xie, X. *Phys. Rev. Lett.* **93**(18), 180603 October (2004).
 - [16] Kou, S. *Annals of Applied Statistics* **2**, 501–535 (2008).
 - [17] Magdziarz, M. and Klafter, J. *Phys. Rev. E* **82**(1), 011129 July (2010).
 - [18] Weber, S. C., Thompson, M. A., Moerner, W. E., Spakowitz, A. J., and Theriot, J. A. *Biophys. J.* **102**(11), 2443–50 June (2012).
 - [19] Kepten, E., Bronshtein, I., and Garini, Y. *Phys. Rev. E* **87**(5), 052713 May (2013).
 - [20] Meroz, Y., Sokolov, I. M., and Klafter, J. *Phys. Rev. Lett.* **110**(9), 090601 February (2013).
 - [21] Bickel, P. J., Ritov, Y., and Stoker, T. M. *Ann. Stat.*

- 34**(2), 721–741 April (2006).
- [22] Berglund, A. J. *Phys. Rev. E* **82**(1), 011917 July (2010).
 - [23] Aït-Sahalia, Y., Fan, J., and Xiu, D. *J. Am. Stat. Assoc.* **105**(492), 1504–1517 December (2010).
 - [24] Michalet, X. and Berglund, A. *Phys. Rev. E* **85**(6), 061916 June (2012).
 - [25] Zhang, L., Mykland, P., and Ait-Sahalia, Y. *Journal of the American Statistical Association* **100**, 1394–1411 (2005).
 - [26] Aït-Sahalia, Y. and Jacod, J. *J. Econ. Lit.* **50**(4), 1007–1050 December (2012).
 - [27] Calderon, C. P. *Phys. Rev. E* **88**(1), 012707 April (2013).
 - [28] Duchesne, P., Ghoudi, K., and Remillard, B. *Can. J. Stat.* **40**(3), 447–479 (2012).
 - [29] The drift function in the $H = \frac{1}{2}$ case is motivated by the overdamped Langevin equation; for $H \neq \frac{1}{2}$, a memory kernel is not used; however our interest is in robustly detecting statistical dependence between components regardless of fluctuation dissipation constraints.
 - [30] Hong, Y. and Li, H. *Rev. Fin. Studies* **18**, 37–84 (2005).
 - [31] Tran, P. V., Haycraft, C. J., Besschetnova, T. Y., Turbe-Doan, A., Stottmann, R. W., Herron, B. J., Chesebro, A. L., Qiu, H., Scherz, P. J., Shah, J. V., Yoder, B. K., and Beier, D. R. *Nat. Genet.* **40**(4), 403–10 April (2008).
 - [32] Ott, C. and Lippincott-Schwartz, J. *Curr. Protoc. Cell Biol.* **Chapter 4**(December), Unit 4.26 December (2012).
 - [33] Thompson, R. E., Larson, D. R., and Webb, W. W. *Biophys. J.* **82**(5), 2775–83 May (2002).
 - [34] Michalet, X. *Phys. Rev. E* **82**(4), 041914 October (2010).
 - [35] Enderlein, J., Toprak, E., and Selvin, P. R. *Opt. Express* **14**(18), 8111–20 September (2006).
 - [36] Gahlmann, A. and Moerner, W. E. *Nat. Rev. Microbiol.* **12**(1), 9–22 December (2014).
 - [37] Cinlar, E. *Introduction to Stochastic Processes*. Prentice Hall College Div, (1997).